

Method to Measure Young's Modulus and Damping of Fibers at Cryogenic Temperatures

Introduction

The direct-drive laser approach to inertial confinement fusion (ICF) at the Laboratory for Laser Energetics (LLE) involves the use of high-power laser beams to uniformly compress a target capsule filled with hydrogen isotopes in a spherically symmetric implosion. The use of cryogenic (cryo) targets, filled with fuel and cooled to form an ice layer at ~ 20 K on the capsule's inner surface, results in higher fuel densities and, therefore, higher yields.¹

A typical production cryogenic target assembly is shown in Fig. 138.1. The target shell's outer diameter is ~ 875 μm and,

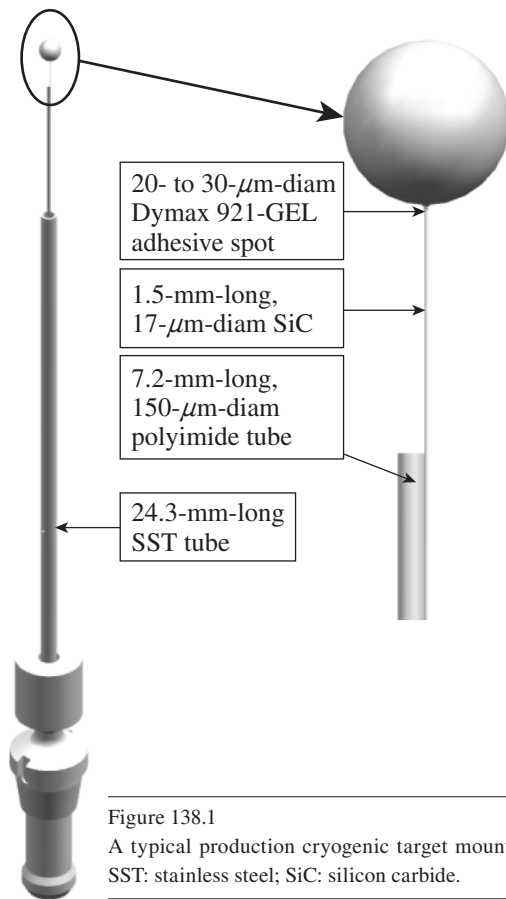


Figure 138.1
A typical production cryogenic target mount assembly.
SST: stainless steel; SiC: silicon carbide.

G10052JR

depending on ice thickness, has a filled mass of ~ 55 μg . The design of cryogenic targets must meet the stringent stability requirement of remaining within 10 μm of target chamber center (TCC) at the time of the shot. Target position is a superposition of static alignment and vibration caused by the retraction of the thermal shrouds that maintain the temperature of the target prior to a shot. When the target offset with respect to TCC is increased, a compression asymmetry is introduced, resulting in a reduction of observed neutron yield.²

Target mount assemblies must be designed with a fundamental mode of >300 Hz at ~ 20 K so that the capsule is minimally excited by the impulse created by the aforementioned shroud retraction. Designing a target mount with a specific natural frequency and transmissibility requires accurate values for Young's modulus and the critical damping ratio at cryogenic temperatures. Data for these material properties at cryogenic temperatures are not available in the literature for the materials of choice in target mount design. The materials of interest for this study are NicalonTM ceramic grade [silicon carbide (SiC)] (Ref. 3), Zylon[®]HM {poly[p-phenylene-2,6-benzobisoxazole] (PBO)} (Ref. 4), M5 {diimidazo-pyridinylene [dihydroxy] phenylene (PIPD)} (Ref. 5), and polyimide.⁶ Table 138.I lists the room-temperature values of Young's modulus taken from the literature for these materials of interest.

The method used in this study involves exciting a target mounted on a fiber of each of these materials over a range of temperatures from ~ 295 K to ~ 20 K. An SiC test target assembly is shown in Fig. 138.2. The experimental setup records the displacement of the target capsule's centroid, caused by an impulse load, with respect to time. From this data, the modulus and damping ratio can be calculated over a range of temperatures. Similar methods have been used to measure Young's modulus in other studies;⁷ however, these tests have not included fiber sample shapes or the materials of interest in this study.

Dynamic mechanical analysis (DMA) is another viable method used to find these parameters; however, the results

Table 138.I: Room-temperature material properties of test target mount materials from the literature.

	Material Form	Density (kg/m ³)	Young's Modulus (GPa)	Outside Diameter (μm)	Inside Diameter (μm)	Active Length of Fiber/Tube (mm)
Nicalon™ (Ref. 3)	fiber	2550	210	17	N/A	2.0
Zylon® HM (Ref. 4)	fiber	1560	270	12	N/A	1.3
M5 (Ref. 5)	fiber	1700	330	12	N/A	1.55
Polyimide (Ref. 6)	fiber	1430	2.5	168	122	7.62
304 Stainless	tube	8000	193	711	483	6.74
Dymax 921-GEL (Ref. 8)	adhesive	1000	2.2	N/A	N/A	N/A
CD strong plasma plastic (Ref. 9)	hollow sphere	1000	2.4	875	827	N/A

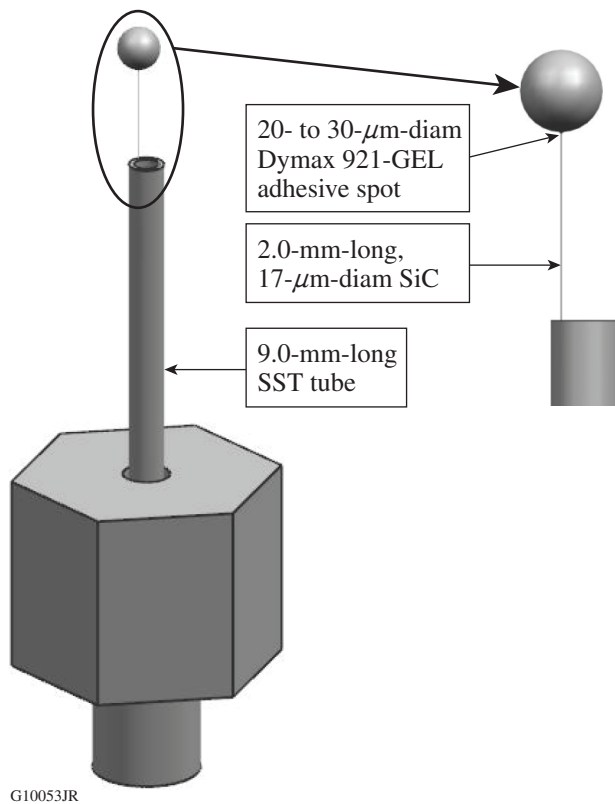


Figure 138.2
A SiC test target assembly used to measure Young's modulus and damping ratio.

are extremely sensitive to the setup and test procedures when measuring fibers <math> < 20 \mu\text{m}</math> in diameter. In addition, it is not possible to reach temperatures below $\sim 100\text{ K}$ (Ref. 10) with the equipment currently available. The method used here demonstrates that these properties can be accurately measured for fiber diameters as small as $12 \mu\text{m}$ at $\sim 20\text{ K}$. Targets with an $\sim 5\text{-}\mu\text{m}$ -diam carbon support have been manufactured at LLE. An extension of this method to these fibers should not present any unique challenges.

Experimental Methods

The Montana Instruments Cryostation¹¹ provides a selectable isothermal environment, from $\sim 295\text{ K}$ down to $\sim 20\text{ K}$, to conduct vibration tests on sample targets. The test setup is shown in Fig. 138.3. A target capsule without fuel is supported by a fiber of the material of interest and cooled in a helium environment to the desired test temperature. Figure 138.4 shows a test target mounted to the internal cryostation support structure. The entire support structure and target are shrouded in helium to maintain an isothermal environment among the support structure, target temperature sensor, and target assembly. The Montana Instruments Cryostation is designed to minimize steady-state target vibrations caused by the presence of its cold-head [$< 25\text{-nm rms}$ (root-mean-square) background vibration]. The test target is excited by an impulse from a modal hammer hit on the body of the cryostation at a given temperature set point. The cryostation's low background vibration contributes to a high signal-to-noise ratio of the target's response to the applied impulse.

Two high-speed cameras with perpendicular viewing angles capture video of target vibrations at a sampling rate of 2000 frames per second. Post-processing software is used to record the displacement of the centroid of the target capsule in each frame, resulting in a displacement (along the x and y axes) versus time data set. Test targets were designed to have a fundamental frequency, at room temperature, of $\sim 3\times$ lower than the Nyquist frequency of the measurement system. The modulus of the fiber is calculated from the fundamental frequency of the target assembly, and damping is calculated from the logarithmic decay of the waveform in the time domain.

Modal hammer hits are aligned with the y axis, and target vibration data are recorded along the x and y axes by using both cameras. A typical vibration response to an impulse aligned

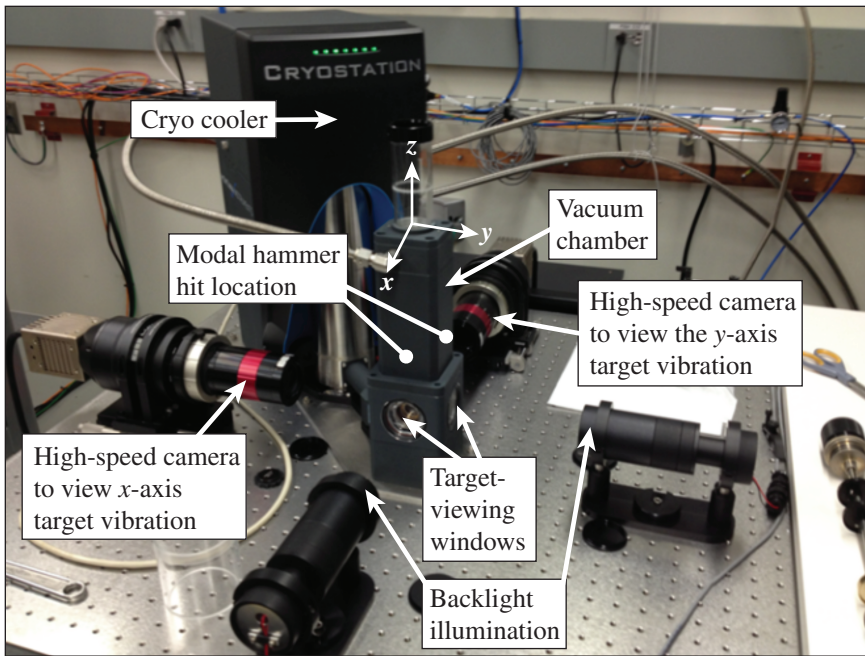
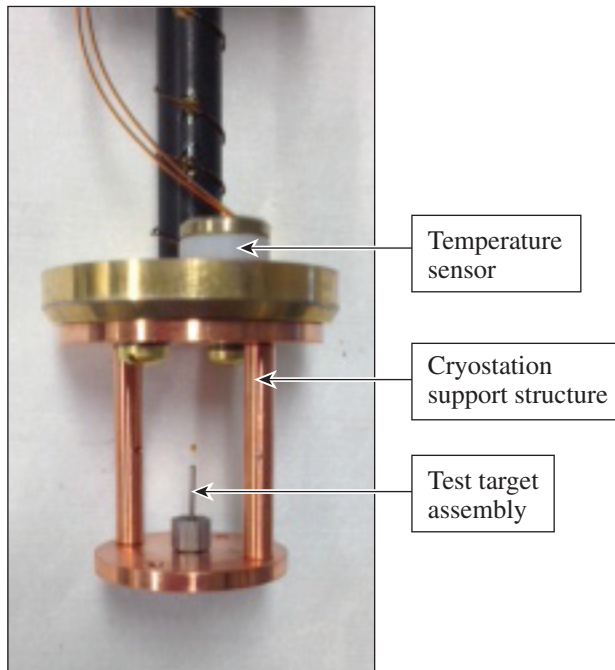


Figure 138.3
Test setup used in this study.

G10054JR



G10055JR

Figure 138.4
Image of a test target mounted to the internal cryostation support structure.

with the y axis is shown in Fig. 138.5 for a SiC fiber test target at 20 K. Damping is measured by the rate of vibration decay in the time domain [Fig. 138.5(a)]. The modulus of the fiber is calculated based on the fundamental vibration mode along the y axis [Fig. 138.5(b)]. The x-axis vibration amplitude is much

lower than the y-axis amplitude since the impulse is directed along the y axis. The x- and y-axes' fundamental modes are 283 Hz and 292 Hz, respectively. The difference is likely due to the fact that the fiber cross section is not perfectly circular. A subsequent impulse aligned with the x axis confirmed that the x-axis fundamental mode is 283 Hz.

Theory

The following equations describe the main theoretical concept of this experimental method: that the fundamental frequency of the test targets can be used to estimate Young's modulus. The natural frequency (f_n) of a cantilevered beam supporting a point mass at its end is proportional to the square root of its modulus (E):¹²

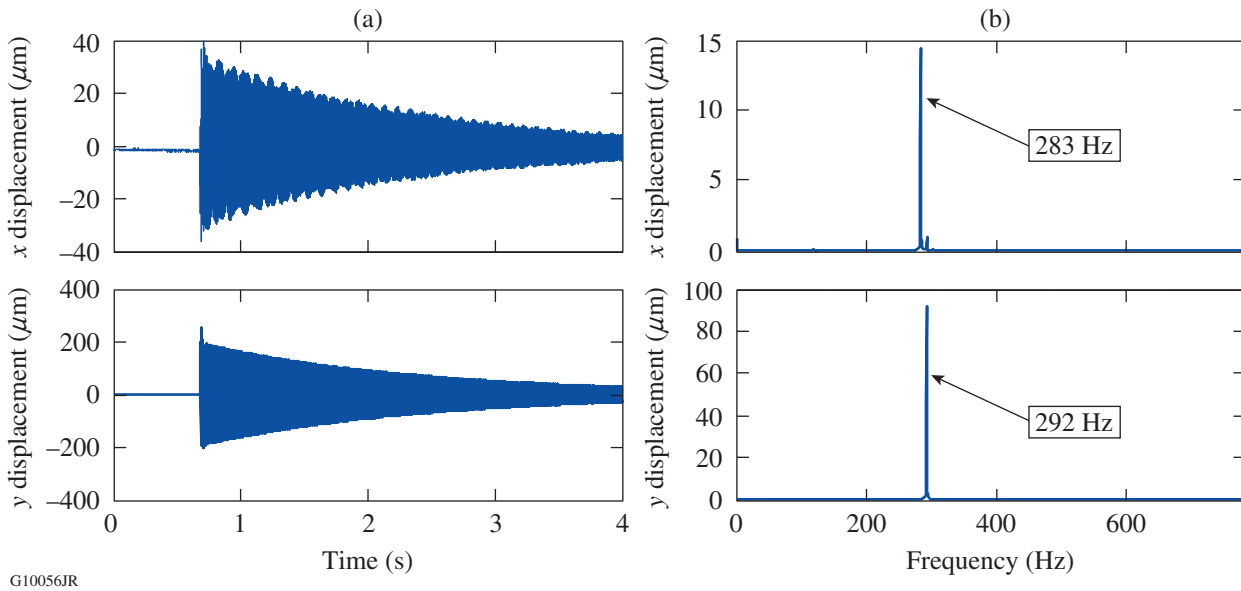
$$f_n = \frac{1}{2\pi} \left[\frac{3EI}{L^3 (M + 0.24 M_b)} \right]^{1/2}, \quad (1)$$

where I is the beam's second area moment of inertia, L is the length of the cantilever beam, M is the point mass supported by the free end of the beam, and M_b is the fiber mass.

Solving Eq. (1) for E yields

$$E = \frac{L^3 (M + 0.24 M_b) (2\pi f_n)^2}{3I}. \quad (2)$$

Using Eq. (2), the modulus can be estimated based on the measured fundamental mode of a cantilever beam structure.



G10056JR

Figure 138.5

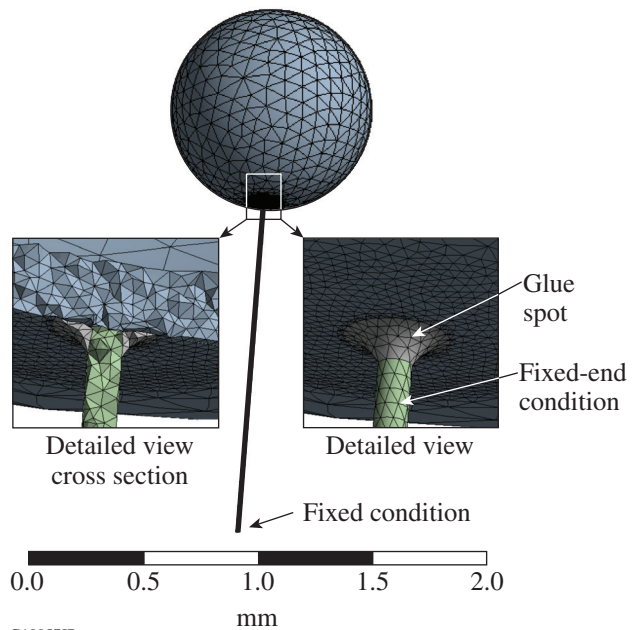
Typical target vibration response data collected in this study for a Niclon™ fiber test. In this case (a) shows target vibration with respect to time and (b) shows the fast Fourier transform (FFT) of target vibration.

As a result of the nature of accounting for only one degree of freedom, this equation does not account for the moment caused by the offset of the point mass at the end of the fiber and the stiffness of the capsule, glue joint, and stainless-steel support tube. Finite element (FE) models are used to account for the additional flexibilities of the studied test target assemblies.

An ANSYS™ one-dimensional (1-D) FE model (beam elements) was used to compute the fundamental mode of each test setup. The target shell was treated as rigid, and its mass and rotational inertia were included using a point mass element. A rigid link, from the end of the fiber to the target's centroid, accounts for the offset of the target's center of gravity. Results from these models show that because of its large cross section relative to the test fiber, the stainless-steel tube's effect on the resulting fundamental frequency is negligible (~0-Hz change) and can be treated as rigid.

An ANSYS™ three-dimensional (3-D) FE model (solid elements) was then created to investigate how the stiffness of the glue joint that connects the target capsule to the fiber and the stiffness of the capsule affect the fundamental frequency of the test target assembly. Figure 138.6 shows the model's mesh, including a detailed view of the glue spot. This model shows that increasing the room-temperature value of Young's modulus of the glue and target capsule by a factor of 10—much greater

than it would experience if cooled down to ~20 K—does not significantly change the fundamental frequency (<3-Hz change) of the system (see columns 3 and 4 of Table 138.II).



G10057JR

Figure 138.6

Three-dimensional finite element (FE) model mesh with details of the glue spot.

Table 138.II: Comparison of finite element (FE) results and test data.

1	First Natural Frequency				Young's Modulus		Fiber Dimensional Change to Match Literature Values	
	2	3	4	5	6	7	8	9
Fiber material	1-D model (Hz)	3-D model (Hz)	3-D model 10× stiffer (Hz)	Test at 295 K (Hz)	Predicted E at 295 K for the 3-D FE model (GPa)	Literature E at 295 K (GPa)	Delta diameter to match literature (μm)	Delta length to match literature (μm)
Nicalon™	287	280	282	288	222	210	0.2	-40
Zylon® HM	271	261	264	241	230	270	-0.4	90
M5	244	233	236	206	258	330	-0.7	150
Polyimide	363	361*	361*	370	2.6	2.5	2.0	-80

*Glue was not included in this model.

Based on the FE models, the stiffness of the stainless-steel tube, glue spot, and target capsule has a minimal effect on the test target's fundamental frequency. Therefore, it can be stated that any change in the test target's fundamental mode as a function of temperature is a result of a change in only the test fiber's modulus.

Columns 3 and 5 of Table 138.II compare 3-D FE model estimates of the test targets' fundamental frequency at room temperature [using modulus values (column 7) from the literature] with test results at room temperature. Column 6 of Table 138.II lists the values of Young's modulus of the test fiber that are required for the 3-D FE model to match test results. Note that the predicted value of the modulus can vary significantly from what is published in literature, especially for Zylon®HM (230 versus 270 GPa) and M5 (258 versus 330 GPa). Columns 8 and 9 provide insight into two possible causes. Fiber diameters used in this study are estimated from microscope images with a 200× magnification. Table 138.I lists the diameters of tested fibers; both Zylon®HM and M5 have a nominal diameter of ~12 μm . Column 8 of Table 138.II lists the change in fiber diameter required for the 3-D FE model to match the fundamental frequency test results. The inferred diameter differences are less than can be resolved by the fiber-diameter measurement technique used here. In addition, if the fiber diameter is left at its nominal value, column 9 lists the change in fiber length required for the 3-D FE model to match the fundamental frequency test results. The sensitivity of the fundamental mode to uncertainties in fiber diameter or length indicates that it is not possible to obtain accurate absolute measurements of Young's modulus with this experimental technique.

However, if an accurate measurement of a test fiber's Young's modulus is available at one test temperature (room temperature in this article) and fundamental frequencies have been measured at multiple temperatures, additional values of the modulus at the measured temperatures can be calculated. Equation (2) shows that for a cantilever beam of constant cross section and modulus, the modulus is proportional to the fundamental frequency squared. Assuming the test fiber's modulus and its test target's fundamental frequency are known at room temperature, the modulus at a different temperature is computed as follows:

$$E^T = E^{RT} \left(\frac{f_n^T}{f_n^{RT}} \right)^2, \tag{3}$$

where E^T is the estimated Young's modulus, E^{RT} is the measured Young's modulus at room temperature (RT), f_n^T is the measured fundamental frequency at temperature of interest, and f_n^{RT} is the measured fundamental frequency at room temperature.

Calculations

As stated in **Experimental Methods** (p. 104), data from the high-speed camera are post-processed, yielding a vibration waveform of the target capsule's centroid displacement. A fast Fourier transform (FFT) of this waveform gives the fundamental mode of the test fiber. Equation (3) is used to compute Young's modulus as a function of temperature. The logarithmic decrement (rate of decay of free vibration) is used to measure the critical damping ratio of the test fiber:¹³

$$\zeta = \frac{\ln(x_1/x_2)}{2\pi N}, \quad (4)$$

where x_1 and x_2 are the magnitudes of two peaks in the time domain and N is the number of cycles between these peaks.

Results

Figure 138.7(a) shows the minimum, equilibrium, and maximum displacements of an actual M5 target assembly vibrating at 20 K. The top of the stainless-steel tube in the images is a fixed reference point (i.e., it does not move). Figure 138.7(b) shows the corresponding images of a FE representation of an M5 target assembly vibrating at 20 K. The top of the stainless-steel tube is fixed to ground in all six degrees of freedom. The mode shape, as one would expect, is the first bending mode of a cantilever beam.

All four test assemblies were tested at multiple temperatures. At each temperature of interest, the target assembly was excited by a modal hammer hit on the exterior of the cryostat and the resulting target vibrations were recorded. Three measurements at each temperature were recorded. Using Eq. (3) and published values of Young's modulus at room temperature, the modulus at the test temperature was determined. Table 138.III lists the average (of the three measurements taken) fiber modulus at each temperature tested. Using Eq. (4), the critical damping ratio was calculated for each test point. The averages of the three measurements at each temperature are listed in Table 138.IV. Figures 138.8 and 138.9 show plots of the modulus and critical damping ratio, respectively, versus temperature.

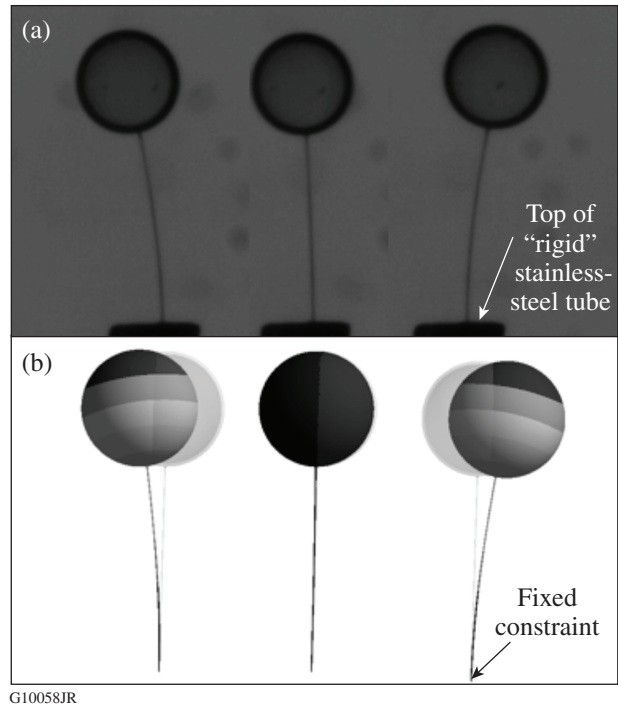


Figure 138.7 Comparison of (a) test image and (b) FE model mode shapes for the M5 target test assembly at 20 K.

In both figures, the markers represent the average value and the error bars represent the range of measurements. (Note that the modulus of polyimide is given by the right ordinate axis in Fig. 138.8.)

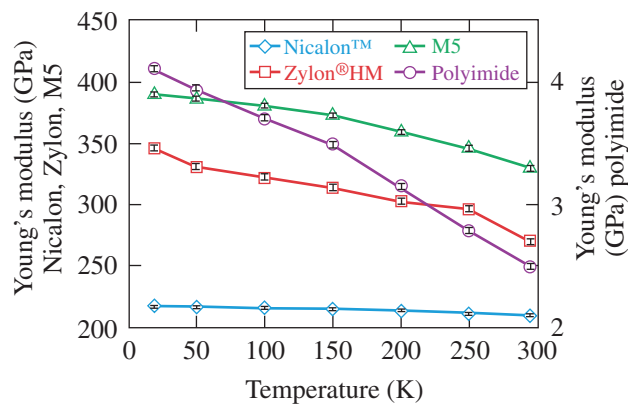
Table 138.III: Experimental values of Young's modulus for each fiber material in GPa measured at various temperatures.

	20 K	50 K	100 K	150 K	200 K	250 K	295 K*
Nicalon™	217	217	216	216	214	212	210
Zylon® HM	346	331	323	314	303	297	270
M5	390	387	381	373	359	346	330
Polyimide	4.1	3.9	3.7	3.5	3.1	2.8	2.5

*The modulus at 295 K taken from literature.³⁻⁶

Table 138.IV: Experimental values of the critical damping ratio for each fiber material in GPa measured at various temperatures.

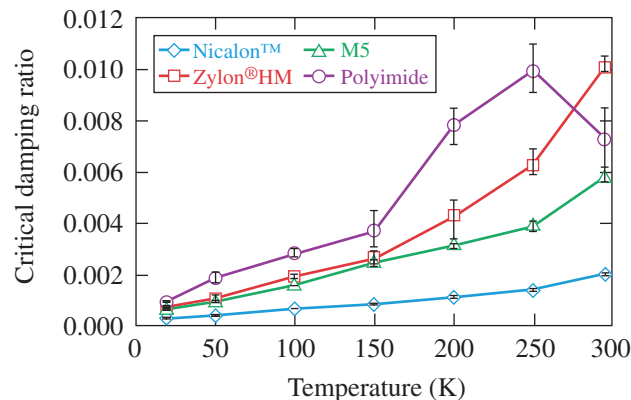
	20 K	50 K	100 K	150 K	200 K	250 K	295 K
Nicalon™	0.00031	0.00046	0.00070	0.00089	0.00113	0.00143	0.00207
Zylon®HM	0.00072	0.00107	0.00197	0.00263	0.00430	0.00630	0.01013
M5	0.00068	0.00099	0.00160	0.00253	0.00313	0.00390	0.00583
Polyimide	0.00096	0.00187	0.00280	0.00370	0.00783	0.00993	0.00730



G10059JR

Figure 138.8

Young's modulus of test fibers as a function of temperature (note the modulus of polyimide is given by the right ordinate axis).



G10060JR

Figure 138.9

Critical damping ratio of test fibers as a function of temperature.

Conclusions

The experimental method used in this article allows one to accurately measure Young's modulus and the critical damping ratio for fiber diameters as small as $12\ \mu\text{m}$ at $\sim 20\ \text{K}$. Significant changes are seen in Young's modulus—stiffer at lower temperatures—for the three polymeric fibers with respect to temperature, while Young's modulus is relatively invariant to temperature for the ceramic fiber. Significant changes in the critical damping ratio—less damping at lower temperatures—are seen for all four fibers with respect to temperature. Below 50 K, all four fibers have a critical damping ratio of less than 0.002. This low-damping level makes it extremely difficult to design low-vibration cryogenic targets because of their high transmissibility.

ACKNOWLEDGMENT

This material is based upon work supported by the Department of Energy National Nuclear Security Administration under Award Number DE-NA0001944, the University of Rochester, and the New York State Energy Research and Development Authority. The support of DOE does not constitute an endorsement by DOE of the views expressed in this article.

REFERENCES

1. P. W. McKenty, T. C. Sangster, M. Alexander, R. Betti, R. S. Craxton, J. A. Delettrez, L. Elasky, R. Epstein, A. Frank, V. Yu. Glebov, V. N. Goncharov, D. R. Harding, S. Jin, J. P. Knauer, R. L. Keck, S. J. Loucks, L. D. Lund, R. L. McCrory, F. J. Marshall, D. D. Meyerhofer, S. P. Regan, P. B. Radha, S. Roberts, W. Seka, S. Skupsky, V. A. Smalyuk, J. M. Soures, K. A. Thorp, M. Wozniak, J. A. Frenje, C. K. Li, R. D. Petrasso, F. H. Séguin, K. A. Fletcher, S. Padalino, C. Freeman, N. Izumi, J. A. Koch, R. A. Lerche, M. J. Moran, T. W. Phillips, G. J. Schmid, and C. Sorce, *Phys. Plasmas* **11**, 2790 (2004).
2. S. X. Hu, V. N. Goncharov, P. B. Radha, J. A. Marozas, S. Skupsky, T. R. Boehly, T. C. Sangster, D. D. Meyerhofer, and R. L. McCrory, *Phys. Plasmas* **17**, 102706 (2010).
3. NICALON™ Ceramic Fiber (Rev. 1/06), COI Ceramics, Inc. (an ATK Space Systems affiliate), Magna, UT 84044 (http://www.coiceramics.com/pdfs/Nicalon_1-17-06.pdf).
4. PBO Fiber Zylon®, Technical Information (Revised 2005.6), Toyobo Co., Ltd. (http://www.toyobo-global.com/seihin/kc/pbo/Technical_Information_2005.pdf), p. 3.
5. M. Afshari, R. Kotek, and P. Chen, in *High Performance Polymers and Engineering Plastics*, edited by V. Mittal (Scrivener Publishing, Salem, MA, 2011), Chap. 9, pp. 269–340.
6. Properties of DuPont VESPEL® Parts, DuPont Engineering Polymers, Newark, DE 19714-6100 (<http://www.craftechind.com/assets/Vespel-Dupont.pdf>), p. 6.
7. W.-H. Chuang *et al.*, *J. Microelectromech. Syst.* **13**, 870 (2004).
8. Dymax® 921-GEL Product Data Sheet (Rev. 06/27/12), Dymax Corporation, Torrington, CT 06790 (<http://www.dymax.com/images/pdf/pds/921-gel.pdf>).
9. A. Nikroo *et al.*, *Fusion Sci. Technol.* **45**, 229 (2004).
10. DMA 8000, PerkinElmer, Waltham, MA 02451 (http://www.perkinelmer.com/CMSResources/Images/44-74431BRO_DMA8000.pdf).
11. Cryostation, Montana Instruments, Bozeman, MT 59715 (<http://www.montanainstruments.com/docs/Cryostation-Catalog.pdf>).
12. R. D. Blevins, *Formulas for Natural Frequency and Mode Shape* (Van Nostrand Reinhold Co., New York, 1979).
13. W. T. Thomson, *Theory of Vibration with Applications*, 2nd ed. (Prentice-Hall, Englewood Cliffs, NJ, 1981).